# Experimental analysis and optimization of the variable valve timing on attaining high efficiency with low NOx emission of a direct-injected hydrogen engine

**Feng-yu Lai [a], Bai-gang Sun [a, b], Shi-wei Zhang [a], Kang-da Wang [a], Qing-he Luo [a, b], Ling-zhi Bao [a,c *], Felix Leach [c]**

a School of Mechanical Engineering, Beijing Institute of Technology, Beijing 100081, China

b Beijing Institute of Technology Chongqing Innovation Center, Chongqing, 401121, China

c Department of Engineering Science, University of the Oxford, Oxford, OX1 3PJ, UK

Corresponding: Ling-zhi Bao (Email: paul.bao@eng.ox.ac.uk)

## Abstract

The direct-injection hydrogen engine (DI-$H_2$ICE) has demonstrated zero carbon emissions with high brake thermal efficiencies (BTE). Due to the high stoichiometric air-fuel ratio of hydrogen, with a lean burn strategy the gas exchange process of a hydrogen engine is different to a gasoline engine, and the valve timing controlling strategy requires reinvestigation. In this research, the optimal variable valve timing (VVT) is investigated in a 2.0 L DI $H_2$ICE. The intake and exhaust valve timing controlling strategies are analyzed experimentally over the whole operating map. A multi-indicator decision-making method is applied to determine the entropy weight of BTE and NOx emissions. Results indicate that BTE greatly benefits from advanced intake valve timing, and exhaust valve timing affects BTE through pumping losses. Advanced intake and exhaust valve timings are employed in the hydrogen engine to enhance the BTE until the NOx emissions rise rapidly at high loads. The retarded exhaust valve timing helps reduce NOx emissions and avoid the risk of abnormal combustion at high loads. Therefore, earlier IVO and later EVC are applied simultaneously for DI-$H_2$ICE compared to the gasoline engine. A maximum power of 124.8 kW at an engine speed of 4500 rpm and a BTE of 42.57% is achieved with optimized VVT. Furthermore, NOx emissions are controlled to under 20 ppm over nearly half of the engine operating map. The conclusions are valuable in the development of high-performance $H_2$ICEs, the numerical simulation studies, and hydrogen fuel applications.

**Keywords:** hydrogen engine; Miller cycle; VVT optimization;

**Nomenclature:**

| | |
|---|---|
| $H_2$ICE | hydrogen engine |
| HFC | hydrogen fuel cell |
| PFI | port fuel injection |
| DI | direct injection |
| SOI | start of injection |
| VVT | variable valve timing |
| VGT | variable geometry turbine |
| IVO | intake valve opening |
| EVC | exhaust valve closing |
| λ | excess air ratio |
| BMEP | brake mean effective pressure |
| BTE | brake thermal efficiency |
| CR | compression ratio |
| MBT | minimum spark advance for best torque |
| ST | spark timing |
| HRR | heat release rate |
| BD 0-10 | delay period |
| BD 10-90 | burn duration |
| BSFC | brake specific fuel consumption |
| PMEP | pumping effective mean pressure |
| PMEP/IMEP | pumping loss ratio |
| $P_{IVO}$ | cylinder pressure at IVO |
| $P_{EVC}$ | cylinder pressure at EVC |
| bTDC | before top dead center |
| aTDC | after top dead center |

## 1. Introduction

The development of clean renewable fuels is a significant issue currently due to pollutant emissions, climate change, and the lack of fossil resources [1–3]. Hydrogen, as a renewable and carbon-free fuel, will play a promising role in energy sources and decarbonizing transport in the future [4,5]. Generally, there are two main methods to use hydrogen energy: hydrogen engines ($H_2$ICEs) [6] and hydrogen fuel cells [7]. $H_2$ICEs have a higher power density, a lower manufacturing cost, and a lower fuel purity requirement [8–11] compared to fuel cells, therefore $H_2$ICEs will still play a key role in the near future [12].

Additionally, hydrogen, as a fuel in internal combustion engines, has many benefits including wide ignition limits, fast burning velocity, high thermal efficiency, and a high heating value [9,13,14]. Hydrogen addition in traditional or alternative fueled engines has been investigated by many researchers [15–17], and it benefits combustion stability and the lean burn limit. However, the performance needs to be optimized while maintaining the same power level as in a diesel engine [18], which creates additional requirements for combustion and turbocharging [19]. Currently, higher power density, higher thermal efficiency, and lower NOx emissions are always the desired goals of researchers - such as the maximum power of 120 kW, maximum torque of 340 N·m, and maximum brake thermal efficiency (BTE) of 42.63% achieved by Bao et.al [20]. Even though the power and economic performance of DI are better than that of the PFI, the numerical research of Lu et. al [21] noted that the NOx emissions of a PFI 0.86L hydrogen engine, is as low as 0.2g/kWh, compared to that of a DI hydrogen at 2.11 g/kWh. In addition, the after-treatment of hydrogen engines to minimize NOx emission has been investigated. Özyalcin et. al [22] observed that Copper-based SCR catalysts have an early light-off temperature and reach maximum efficiencies of up to >99%, while the vanadium-based SCR provides no secondary $N_2O$ emissions. In this research, various techniques like lean burn, the Miller cycle and turbocharging are employed to reach the maximum BTE. The Miller cycle plays an important role in raising thermal efficiency, and it can be achieved by the technology of variable valve timing (VVT).

VVT is widely employed in conventional (fossil-fuelled) internal combustion engines and the effects of VVT in different fuel engines have been extensively studied. The effect of VVT on a 1.5 L GDI engine was conducted by Yuan et. Al [23]. They reported that when the intake valve timing is advanced by 50°CA, the effective cylinder volume can be increased by 14% and the residual gas fraction increases. Kim et. Al [24] reported that advanced intake valve opening (IVO) leads to increasing airflow because of the negative pressure generated by the discharged exhaust gas according to their test results from a 1.35 L port fuel injection (PFI) turbocharged natural gas engine. In addition, the amount of methane slip climbs when the valve overlap significantly increases, resulting in a loss in thermal efficiency. Shu et.al [25] researched intake valve closing timing strategies on a 9.3 L diesel ignition, natural gas engine by numerical simulation. They reported that the in-cylinder turbulence kinetic energy decreases with retarding the intake valve timing. Basaran et.al [26] investigated the effect on exhaust temperature of VVT on a 6.7 L diesel engine to improve aftertreatment conversion efficiency, and they stated the exhaust temperature can be increased by 60°C while the volumetric efficiency drops from 95% to 63% with retarded intake valve timing. Lee et.al [27] illustrated the impact of VVT on performance experimentally on a 0.5 L PFI supercharged $H_2$ICE. Backfire could be controlled by retarded IVO when the $H_2$ICE power increases to the level of a gasoline engine and the excess air ratio (λ) under normal operation can reach 1. An electric booster with a retarded VVT produced a maximum brake mean effective pressure (BMEP) of 0.912 MPa. Xin et.al [28] studied VVT effects on a 1.5 L PFI hydrogen-enriched ammonia engine, the results showed that increasing the overlap reduces the mixture combustion rate. The BTE dropped from 32.8% to 30% when the intake valve timing was advanced by 5°CA. In addition, a 5°CA advance of intake valve timing caused the coefficient of variation of peak cylinder pressure to rise rapidly from 9.8% to 25%. Verhelst et.al [29] tested different intake valve timings on a 1.78 L PFI bi-fuel hydrogen/gasoline engine. The results showed that a richer mixture ($\lambda$=1) cannot be attained at much advanced intake valve timing due to backfire. Higher overlap leads to higher volumetric efficiency at low and medium speeds. However, at high speeds, a compromise between using exhaust gas inertia with an early intake valve timing and using fresh charge inertia with a late intake valve timing is necessary. Park et.al [30] pointed out that the exhaust valve timing of a 2.36 L PFI naturally aspirated $H_2$ICE is related to the pumping loss, and the retarded intake valve timing reduces output torque because of backfire. Therefore, it can be concluded that VVT settings of PFI $H_2$ICE, especially the intake valve timing, is restricted by backfire and the fuel slip, hence further increases in output power performance are always limited.

In addition to PFI $H_2$ICEs, there is another main type of $H_2$ICEs which are direct injection (DI). PFI $H_2$ICEs are more easily and cheaply transformed from the other fuel types [31], but DI is the development trend of $H_2$ICE in the future because of the occurrence of backfire, primarily in PFI $H_2$ICEs [32–34]. In addition, hydrogen takes up approximately 30% of the cylinder volume at a stoichiometric air-fuel ratio because of the low density of hydrogen [35]. Therefore, the output power of PFI $H_2$ICEs decreases by about 30% compared to DI $H_2$ICEs. In contrast, DI $H_2$ICEs can make up for the power loss by avoiding displacement of intake air. In addition, retarded start of injection (SOI) and a stratified mixture can be achieved and these techniques lead to an increase in thermal efficiency. Bao et. al [20] showed VVT effects on a 2.0 L DI turbocharged $H_2$ICE. An increase of BTE of about 1.8% was reached by optimizing VVT, and a maximum BTE of 42.63%

was attained. In addition, a maximum BTE of 41.2% at 2000 rpm and 2500 rpm was be reached with the near-zero emissions [36]. Early intake valve opening resulted in a decrease of airflow, and the best intake valve opening was -20°CA. The best exhaust valve closing was set at -20°CA to balance the work capacity and losses in the exhaust. Ji et. al [37] investigated VVT timing effects on a 1.5 L DI naturally aspirated $H_2$ICE, and achieved 42.22% BTE by optimizing VVT. The combustion duration and cycle variation were altered by IVO and exhaust valve closing (EVC) timing due to the change in mixture distribution and residual gas fraction. The research of Hong et. al [38] stated the BTE can reach a maximum of 43.15% after a 1.5 L DI naturally aspirated $H_2$ICE was tested. Pumping losses and fast, stable combustion, which can be controlled by IVC and EVO timing, play a significant role in the process of achieving high thermal efficiency. Other research by Hong et. al [39] investigated the effect of advanced intake valve timing on an ammonia / hydrogen dual-fuel engine, showing that earlier intake valve timing leads to an inferior combustion process.

VVT settings for the highest BTE at a certain load are investigated from systematic tests in previous studies. However, simultaneous high-power and low emissions are necessary for the adoption of $H_2$ICEs. The evaluation of VVT on fuel consumption and emission characteristics under a wide load range was conducted on a traditional engine in some previous studies [40,41]. Due to the properties of hydrogen and the lean burn demand, $H_2$ICE VVT settings suited for whole working condition is essential to be investigated. The challenge of turbocharging could result in low power density and limit the VVT range of $H_2$ICE in previous research. $H_2$ICE turbocharging challenges result from the vast flow range at different engine speeds and the variable geometry turbine (VGT) turbocharger could regulate air flow rate at a wide range with decreasing back pressure at high speeds.

In the present work, a 2.0 L DI turbocharged $H_2$ICE with a VGT is tested. The effects of intake and exhaust valve timing are investigated to attain high power and high thermal efficiency. In addition, the Entropy Weight Method, which is a multi-indicator decision-making method [42], is employed in this research to reveal the optimized direction. The VVT settings across the entire engine operating map are optimized and the difference between gasoline and hydrogen engines is discussed.

## 2. Materials and Methods

### 2.1 Test bench

The test engine is a 2.0 L four-cylinder side-injected DI turbocharged $H_2$ICE with a VGT turbocharger, which was modified from a gasoline engine. The IVO and EVC refer to the crank angle at 0.5mm valve lift. As shown in Figure 1 (a) and (b), the possible variation range of IVO is 42°CA before top dead center (bTDC) to 18°CA after top dead center (aTDC), and the possible variation range of EVC covers from 27°CA bTDC to 17°CA aTDC. The reduced flow range of the turbo is displayed in Figure 1 (c), and the maximum reduced flow rate reaches 0.02 kg/s·K^0.5/kPa.

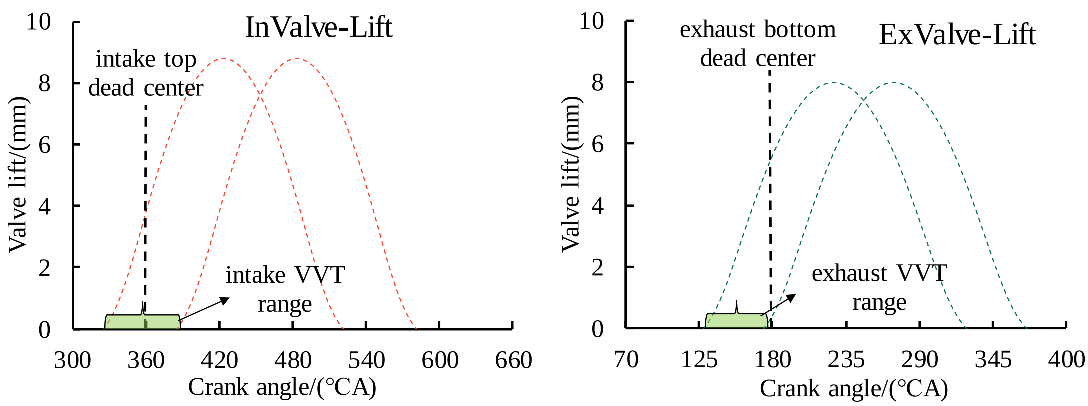


a) Intake valve lift and VVT range b) Exhaust valve lift and VVT range

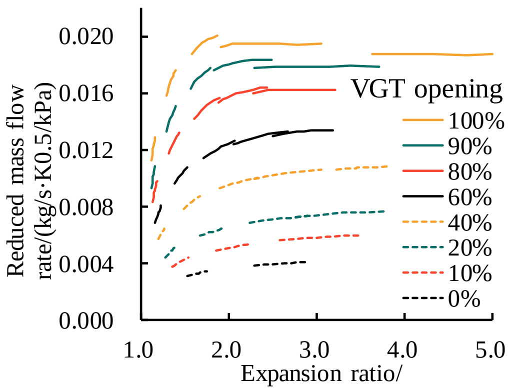


c) The reduced flow rate range of VGT

Figure 1 The valve lift and VGT reduced flow rates of the DI $H_2$ICE

The specifications of the $H_2$ICE are shown in Table 1 and the sketch of the arrangement in the cylinder is displayed in Figure 2 (a). The layout of the experiment and data acquisition systems are shown in Figure 2 (b) and (c).

Table 1 Specifications of the DI $H_2$ICE

| Items | Unit | Values |
|---|---|---|
| Number of cylinders | | 4 |
| Bore | mm | 80.5 |
| Stroke | mm | 98 |
| Displacement | L | 2.0 |
| Number of valves | | 4 |
| Compress ratio | | 12.5 |
| Range of IVO | °CA | 35 bTDC-15 aTDC |
| Range of EVC | °CA | 35 bTDC-10 aTDC |
| Intake valve opening duration | °CA | 196 |
| Exhaust valve opening duration | °CA | 196 |

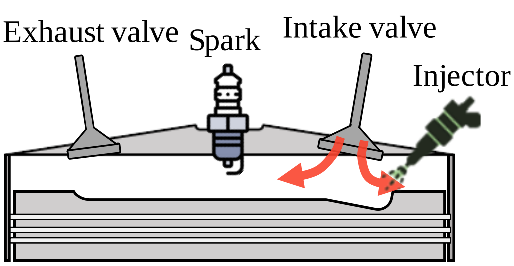


a) Sketch of arrangement in the cylinder

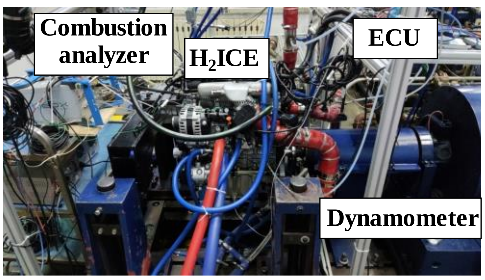


b) Experimental system

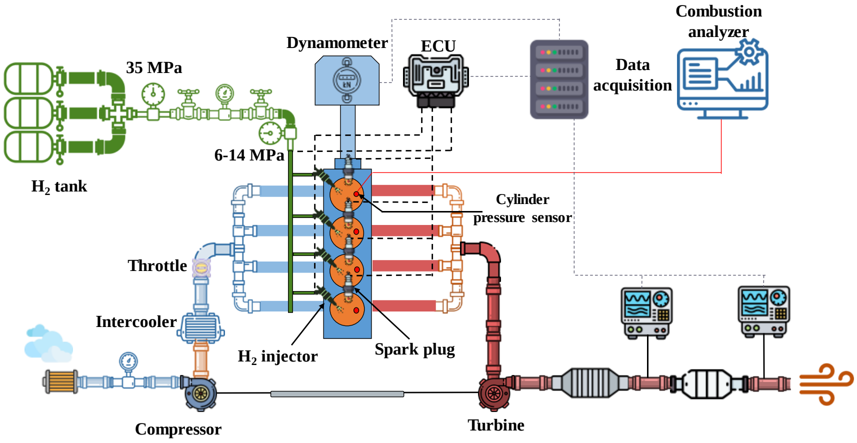


c) Layout of the 2.0 L DI H2ICE experiment and data acquisition systems

Figure 2 Layout of 2.0 L DI H2ICE and experiment/data acquisition systems

The test system contains a CW250 dynamometer with a maximum working capacity of 250 kW and a maximum speed of 8000 rpm. The temperature of the oil and cooling water in the engine is controlled by oil and water temperature controllers. The air mass flow into the engine is measured with MTR-500 Air flowmeters, and an Emerson CMF010 Coriolis mass flow meter is used to determine the hydrogen mass flow. A Kibox combustion analyzer is used in the data acquisition system and the cylinder pressure is recorded with a Kistler 6052C transducer sensor. The specifications of uncertainties of the measured parameters are listed in Table 2. The engine was warmed up before the testing to ensure that the oil and coolant reached 90°C and 80°C, respectively.

Table 2 The measuring devices and data accuracy

| Parameters | Device | Accuracy |
|---|---|---|
| Speed | GW250 dynamometer | ±1 rpm |
| Torque | FC2000 Torque transducer | ±1 N·m |
| Pressure | Kistler 6052C transducer | ±0.02 MPa |
| Air mass flow | MTR-500 Air flowmeters | ±2.5 kg/h |
| Hydrogen mass flow | CMF010 H2 flowmeters | ±0.01 kg/h |
| NOx emissions | AVL DiTEST GAS 1000 | ±3 ppm |

Tests were carried out at the minimum spark advance for best torque MBT (MBT). After the H2ICE operated steadily at the desired test point for 2 minutes, the average value of the test data of 220 cycles at this working condition was measured and recorded.

## 2.2 The Entropy Weight analysis

The Entropy Weight Method is a multi-indicator decision-making method for determining the weights of indicators, which takes into account the relative entropy value between indicators and can better deal with the correlation and difference between indicators [42]. The normalized positive and negative correlation indicators for thermal efficiency and emissions are calculated as the equation below.

$$X_{ij} = \frac{Z_{ij} - min\, Z_{ij}}{max\, Z_{ij} - min\, Z_{ij}} \tag{1}$$

$$X_{ij}{}' = \frac{max\, Z_{ij} - Z_{ij}}{max\, Z_{ij} - min\, Z_{ij}} \tag{2}$$

$$i = 1,2,3, \dots, m \quad j = 1,2,3, \dots, n$$

where $X_{ij}$ and $X_{ij}{}'$ are normalized positive and negative correlation indicators. $Z_{ij}$ is the value of the i$^{th}$ sample and the j$^{th}$ indicator. The max $Z_{ij}$ and min $Z_{ij}$ are the maximum and minimum values in the j$^{th}$ indicator.

The weight of each sample value $P_{ij}$ can be calculated as

$$P_{ij} = \frac{X_{ij}}{\sum_{i=1}^{n} X_{ij}} \qquad j = 1,2,3, \dots, n \tag{3}$$

The information entropy value $l_j$

$$l_j = -\frac{\sum_{i=1}^{m} X_{ij} \ln X_{ij}}{ln\, m} \qquad j = 1,2,3, \dots, n \tag{4}$$

Calculate the weight of the j$^{th}$ indicator $\omega_j$

$$\omega_j = \frac{1 - l_j}{n - \sum_{i=1}^{n} l_j} \qquad j = 1,2,3, \dots, n \tag{5}$$

The evaluation of each sample can be calculated as the equation below:

$$Evaluation_i = \sum_{j=1}^{n} \omega_j X_{ij} \quad j = 1,2,3, \dots, n \tag{6}$$

# 3. Results and Discussions

### 3.1 Entropy Weight analysis of the thermal efficiency and the $NO_x$ emissions

As shown in Figure 3 (a) and (b), the effects of IVO and EVC at different loads on pumping loss and air flow are investigated based on results of sweeps, where the BMEP ranges from 0.62 MPa to 0.64 MPa at 2500 rpm. However, it is hard to determine the optimal VVT settings after a detailed sweep because a maximum BTE of 38.93% is achieved with IVO = -35°CA and EVC = -10°CA in Figure 3 (c), while the zero $NO_x$ emissions are reached with retarded IVO and EVC in Figure 3 (d). Hence, it is worth applying the entropy weight method to evaluate the optimal VVT settings with balanced efficiency and emissions performance.

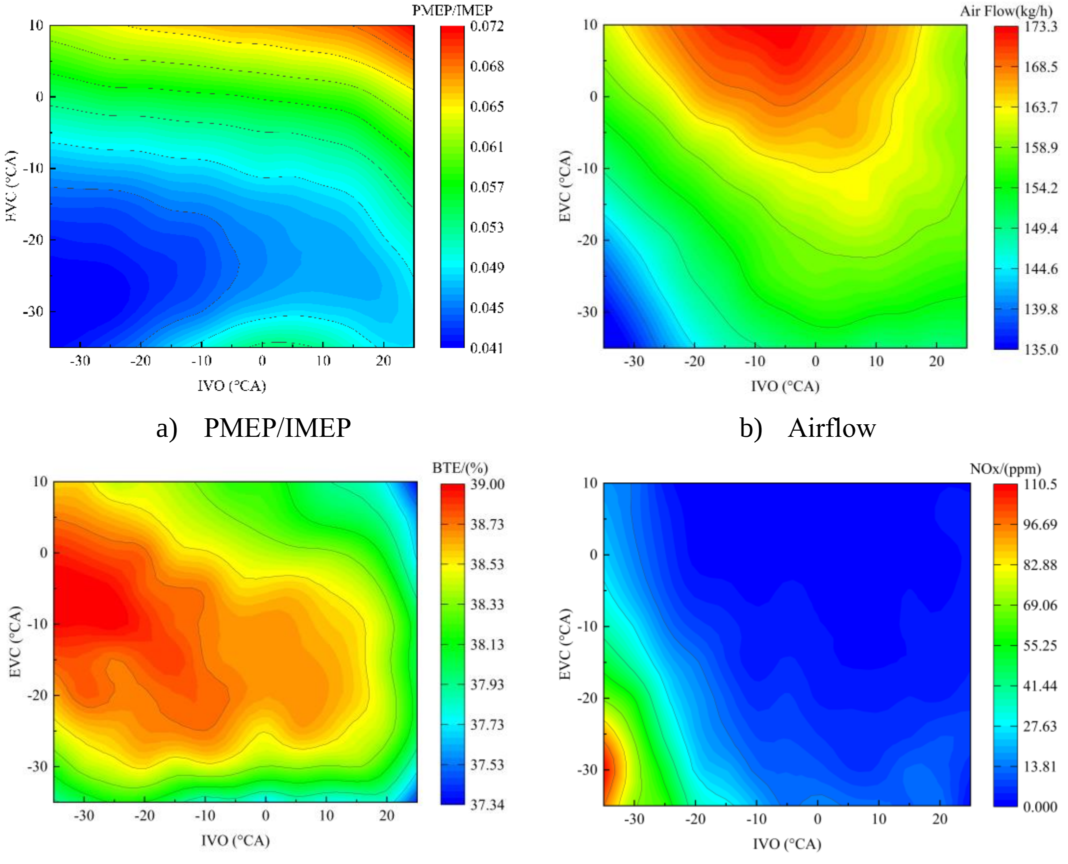


a) PMEP/IMEP

b) Airflow

c) BTE

d) $NO_x$ emission

Figure 3 Effect of VVT on a) PMEP/IMEP, b) Airflow, c) BTE air flow and d) $NO_x$ emissions at 2500 rpm with BMEP ranging from 0.62 MPa to 0.64 MPa

The Entropy Weight analysis is focused on the evaluations of thermal efficiency and $NO_x$ emissions and the calculated results are listed in Table 3. The weight of thermal efficiency is significantly higher than that of NOx emissions at low loads with various engine speeds, indicating a higher BTE is supposed to be the first goal. Furthermore, the Entropy weight of NOx emission climbs as the engine speed increases.

Table 3 Weight of thermal efficiency and NOx emissions at different engine speeds

| Engine speed/(rpm) | BMEP/(MPa) | Weight of thermal efficiency/% | Weight of NOx emissions/% |
|---|---|---|---|
| 2000 | 0.89 | 95.7 | 4.3 |
| 3000 | 0.94 | 90.8 | 9.2 |
| 4500 | 0.77 | 85.8 | 14.2 |

The weights of the two indicators also change with the increasing BMEP. Calculations are obtained according to the test results at 2500 rpm with different loads. Table 4 shows the weight of thermal efficiency decreases from 96.0% to 27.4%, while the weight of NOx emissions rises to 72.6%. The BTE is the primary indicator for optimization at medium-low loads, and the NOx emissions reverse to the major indicator at high loads. Thus, the VVT settings can be evaluated by the change of entropy weight at different engine loads. As shown in Figure 4, the VVT settings are evaluated with the sweeping results according to the weights in Table 4. The variation of evaluation is consistent with that of BTE, and the optimal IVO and EVC, which are -35°CA and -10°CA respectively, are supposed to be implemented at this state.

Table 4 Weight of thermal efficiency and NOx emissions at different loads with 2500rpm

| Engine speed/(rpm) | BMEP/(MPa) | Weight of thermal efficiency/% | Weight of NOx emissions/% |
|---|---|---|---|
| 2500 | 0.2-1.1 | 96.0 | 4.0 |
| | 1.1-1.6 | 50.8 | 49.2 |
| | 1.6-2.05 | 27.4 | 72.6 |

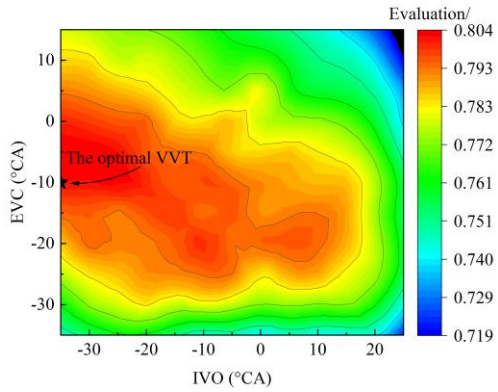


Figure 4 Evaluation of different VVT settings at 2500 rpm

### 3.2 Difference of VVT settings for hydrogen engine

According to Figure 5, the intake pressure with this $H_2$ICE is higher than that of the gasoline engine. The gasoline engine intake pressure is 0.14 MPa when the BMEP is 1.5 MPa, but that of the hydrogen engine exceeds 0.18 MPa at the same BMEP, and the difference grows at low loads. The exhaust back pressure of the hydrogen engine stays at the same level as that of the gasoline engine, and the maximum reaches 0.285 MPa. The comparison displays the advantage of VGT, which is regulating the intake pressure over a wide range with a low exhaust back pressure.

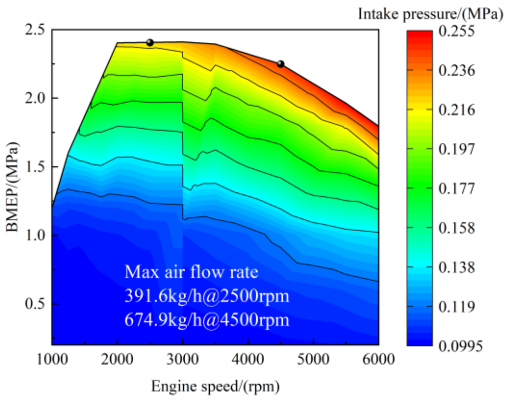


a) Intake pressure of gasoline engine

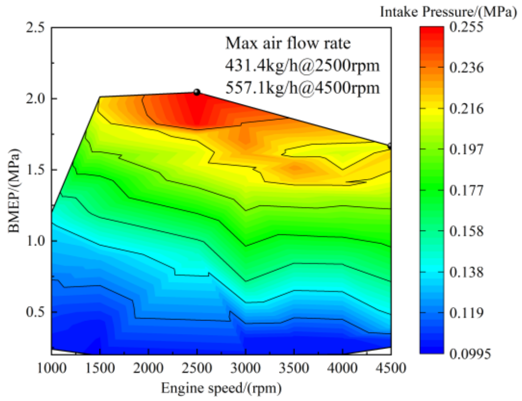


b) Intake pressure of hydrogen engine

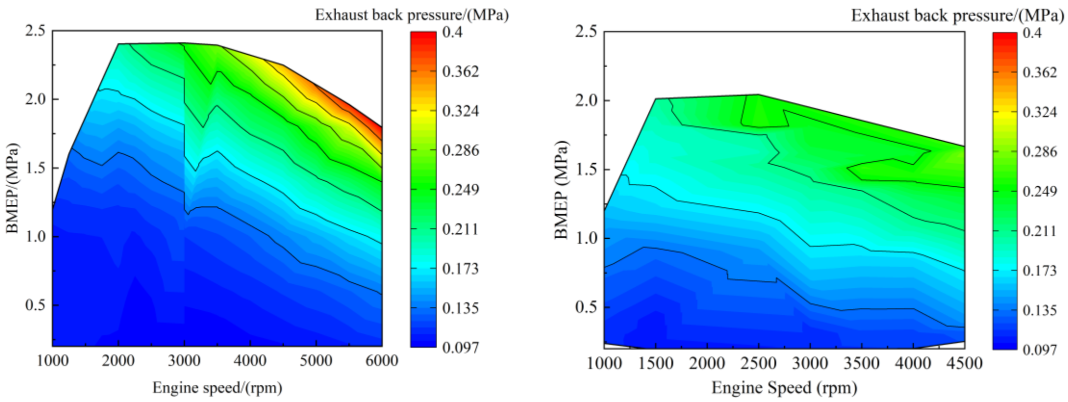


c) Exhaust back pressure of gasoline engine

d) Exhaust back pressure of hydrogen engine

Figure 5 Intake pressure and exhaust back pressure of gasoline engine and hydrogen engine

As seen in Figure 6, the distribution of VVT of gasoline engines is generally located at the earlier IVO and EVC of the VVT range (left bottom of Figure 6) with relatively lower intake pressure. The possible range of IVO is from -35°CA to -5°CA, while the EVC is limited from -35°CA to 0°CA. In contrast, the optimized EVC can be retarded to 10°CA for the hydrogen engine with a higher intake pressure.

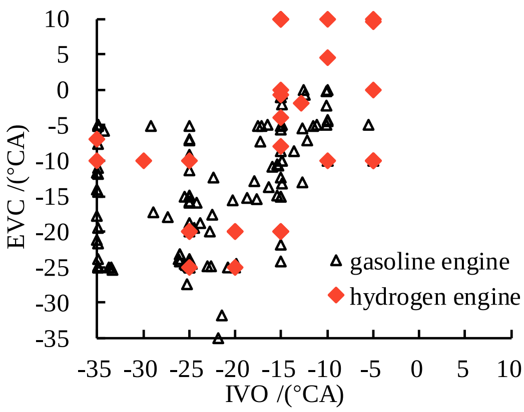


Figure 6 IVO and EVC settings of gasoline and hydrogen engines

The $NO_x$ emissions of the gasoline and hydrogen engines are compared in Figure 7. The results show the hydrogen engine $NO_x$ emissions remain lower at low loads with optimized VVT settings and gradually pass those from the gasoline engine at the highest loads with a maximum of 3656 ppm. Since the weight of $NO_x$ emissions also rises with the increasing load, it is difficult for hydrogen engines to balance the trade-off relationship between the BTE and emissions at high loads.

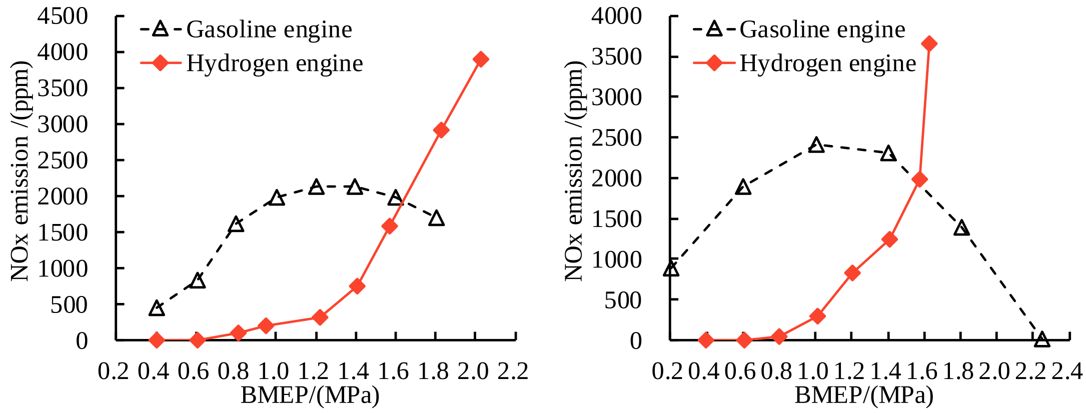


Figure 7 $NO_x$ emissions from the gasoline and hydrogen engines at different engine speeds

Figure 8 shows the VVT controlling strategy of gasoline and hydrogen engines at an engine speed of 1500 rpm and different loads. Both engines adopt the miller cycle which is achieved by advanced intake valve timing at low loads. Residual gas fraction is reduced with slightly advanced exhaust valve time at a low intake pressure. Furthermore, the intake and exhaust valve timing are significantly retarded at high loads to increase the airflow rate. Therefore, the IVOs of the gasoline and hydrogen engines are dramatically advanced at low speeds. Although both gasoline and hydrogen engines use the mildly advanced EVC at low loads and 1500 rpm, the EVC of the gasoline engine is intended to increase airflow due to the low intake pressure below 100kPa, while that of the hydrogen engine is designed for lean burn and low $NO_x$ emissions with sufficient intake pressure - higher than 104.7 kPa. With increasing BMEP, IVO and EVC are retarded to enhance airflow and reduce cylinder residual gases. However, the EVC of hydrogen engines is further retarded to improve airflow and power output. The airflow rate reaches 245.4 kg/h at 2.03 MPa BMEP, whereas the gasoline engine produces 177.0 kg/h at 1.81 MPa BMEP. The sudden retarding of EVC occurs at high loads in the hydrogen engine which is different from the gasoline engine, and it deserves comprehensive discussion. Thus, the effect and strategies of intake and exhaust valve timings on hydrogen engine performance need to be investigated.

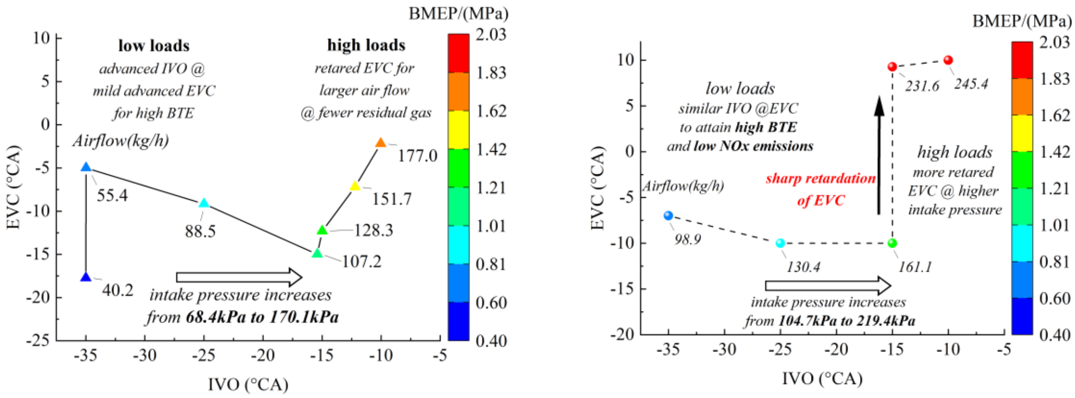


a) Gasoline engine b) Hydrogen engine

Figure 8 VVT settings of gasoline and hydrogen engines at 1500 rpm

### 3.3 Optimized hydrogen engine intake valve timing strategy

The effect of IVO on the hydrogen engine performance is studied first. The tests at different IVOs at 2500 rpm are conducted with EVC fixed at -20°CA. As seen in Figure 9, the λ gradually reduces from 2.32 to 2.13 as the IVO advances from -5°CA to -35°CA at 0.64 MPa BMEP, and λ drops significantly from 2.23 to 1.87 at 0.94 MPa BMEP. Figure 10 (a) shows that the cylinder pressure with advanced IVO is lower than the other cases. In addition, decreasing λ with advancing IVO leads to an increase in heat release rate (HRR) in Figure 10 (b).

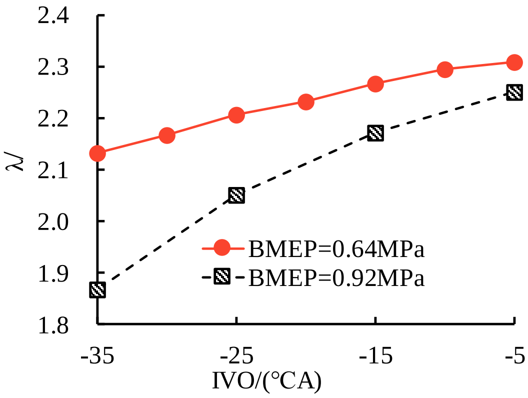


Figure 9 λ variation for different IVOs at 2500 rpm, 0.64 MPa, 0.92 MPa BMEP

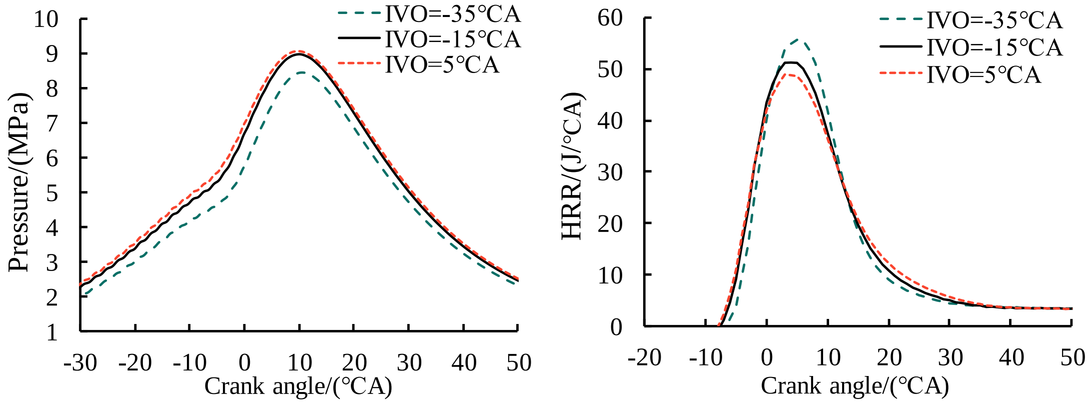


a) Cylinder pressure variations b) HRR variations

Figure 10 Cylinder pressure and HRR variations at 2500 rpm, 0.64 MPa BMEP

Further studies on ignition delay (BD 0-10) and burn duration (BD 10-90) are shown in Figure 11 (a) and (b). At 0.64 MPa BMEP the BD 10-90 reduces from 21.9°CA to 18.6°CA and BD 0-10 drops from 10.0°CA to 9.5°CA as IVO is advanced from -5°CA to -35°CA. Additionally, the BD 10-90 decreases from 22.3°CA to 18.1°CA and BD 0-10 falls from 10.7°CA to 9.4°CA at 0.92 MPa BMEP. This raises the maximum HRR and increases the BTE by improving the degree of constant volume.

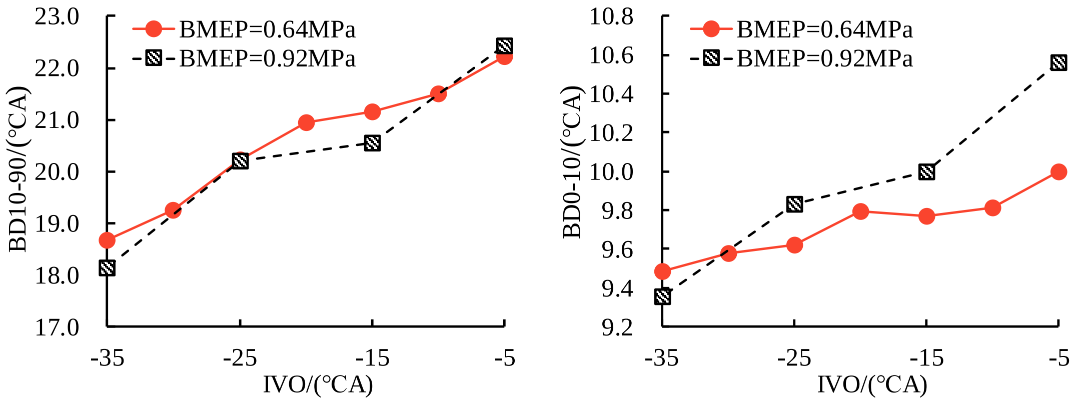


(a) BD 10-90 variations (b) BD 0-10variations

Figure 11 BD 10-90 and BD 0-10 at 2500 rpm, 0.64 MPa BMEP

The optimized IVO at different loads is determined according to the sweeping performance. Figure 12 (a) shows the effect on BTE; when EVC is set at -20°CA, BTE increases continuously from 38.0% to 38.9% as IVO advances from 25°CA to -35°CA at 0.64MPa BMEP, 2500 rpm. In addition, the BTE at 0.92 MPa BMEP climbs from 39.9% to a maximum of 40.4% at -25°CA IVO and then falls to 40.3%. The λ in Figure 9 indicates an optimal lean burn state of -25°CA IVO resulting in an ideal λ of 2.05, but a lower λ is caused by -35°CA IVO. The $NO_x$ emissions are compared at 0.64 MPa and 0.92 MPa BMEP respectively in Figure 12 (b), advanced IVO leads to rapid increases in $NO_x$ emissions. The evaluation is conducted in Figure 13 according to the results of BTE and NOx emissions and it shows the optimal IVO is equal to that of the highest BTE because of the greater weight in thermal efficiency at low loads. The other optimal intake valve timing is selected at different speeds based on the evaluation, and a similar advanced IVO to that of the gasoline engine is implemented.

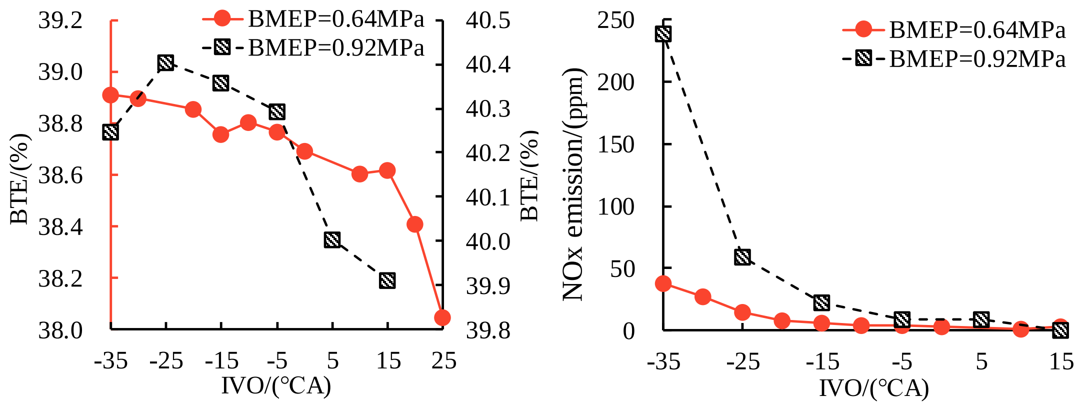


a) BTE variation

b) NOx emissions variation

Figure 12 Performance variation with different IVO at 2500 rpm, 0.64 MPa and 0.92 MPa BMEP

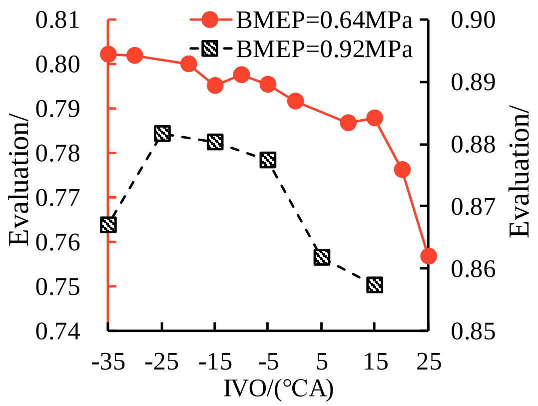


Figure 13 Evaluation of IVO at 2500 rpm, 0.64 MPa and 0.92 MPa BMEP

**3.4 Optimized hydrogen engine exhaust valve timing strategy**

Similarly, the effect of EVC on the hydrogen engine performance is investigated. As shown in

Figure 14 (a), EVC significantly affects the air flow rate and BTE at the same IVO. When the IVO sets at -10°CA, BTE drops from 41.3% to 40.6% as the EVC is retarded from -20°CA to 5°CA, and λ increases from 2.53 to 2.83. The volumetric efficiency climbs from 0.845 to 0.915 and the PMEP/IMEP pumping loss ratio (PMEP/IMEP) increases from 0.027 to 0.053 simultaneously as Figure 14 (b) illustrates.

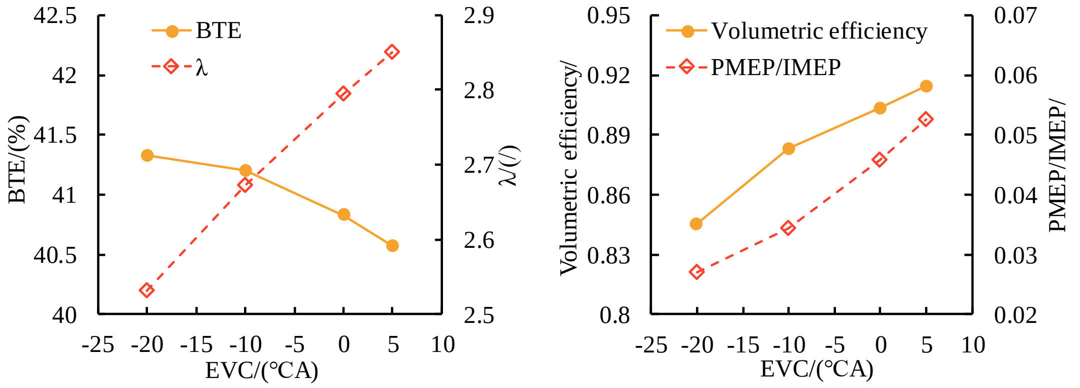


a) BTE and λ at different EVCs

b) Volumetric efficiency and PMEP/IMEP at different EVCs

Figure 14 $H_2$ICE performance parameters at different EVCs

Cylinder pressure at IVO ($P_{IVO}$) gradually declines from 0.282 MPa to 0.265 MPa as EVC is retarded from -20°CA to 5°CA as shown in Figure 15 (a), which has the advantage of reducing the amount of residual gases in cylinder and improving volumetric efficiency. As a result, the retarded EVC leads to higher air flow. Meanwhile, the cylinder pressure at EVC ($P_{EVC}$) also constantly drops from 0.612 MPa to 0.581 MPa as EVC is retarded. The higher $P_{EVC}$ can reduce the gas flow in the exhaust, reducing the pumping loss. As can be observed in Figure 15 (b), the cylinder pressure decreases more rapidly than that at other conditions when EVC is -10°CA.

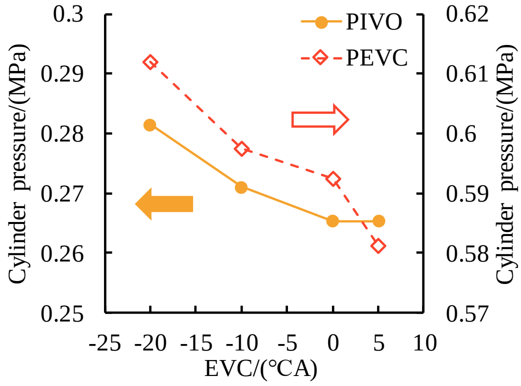


a) $P_{IVO}$ and $P_{EVC}$ at different EVCs

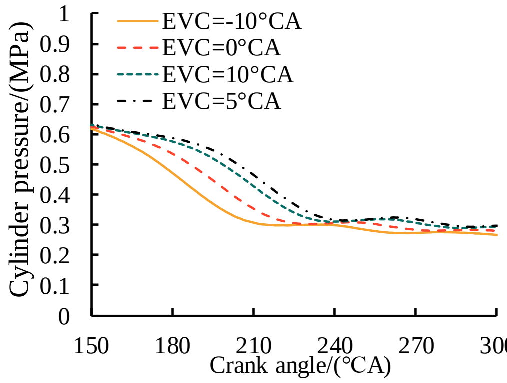


b) Cylinder pressure variation at different EVCs

Figure 15 $H_2$ICE cylinder pressure variations at different EVCs

The optimal exhaust valve timing is investigated at different loads with sweeping tests. The sharp retardation of EVC occurs at 2500 rpm compared to the gasoline engine as seen in Figure 16, and it can be explained as rapid retardation of EVC within a limited range of BMEP. Tests with changed or unchanged VVT settings at 2500 rpm are conducted to investigate the effect of VVT with increasing BMEP. The unchanged IVO and EVC settings are located at -15°CA/-20°CA with decreasing VGT opening, while the EVC of changed VVT settings tests increases from -8°CA to 10°CA. The advanced fixed IVO in changed VVT settings tests is to prevent a sharp decline in BTE.

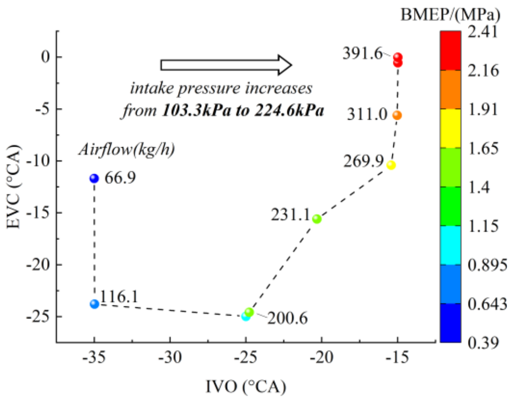


a) Gasoline engine

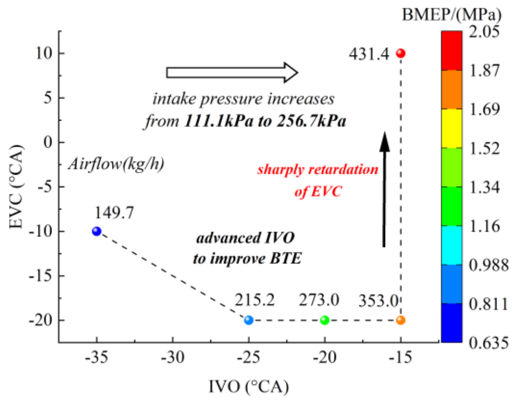


b) Hydrogen engine

Figure 16 VVT settings of gasoline and hydrogen engines at 2500 rpm

According to Figure 17, λ is only controlled by VGT opening at different loads and λ fluctuates greatly. This fluctuation is because of the insufficient control precision of VGT opening. However, λ can be regulated around 2 with changing EVC. Volumetric efficiency constantly increases from 0.82 to 0.95 with retarding EVC. Conversely, the volumetric efficiency remains around 0.82 almost with unchanged VVT, and it gradually drops to 0.78 with the BMEP increasing to 1.74 MPa. This improving volumetric efficiency helps reduce the residual gases in-cylinder and minimizes the risk of abnormal combustion at high loads, highlighting the benefits of retarded EVC at high loads.

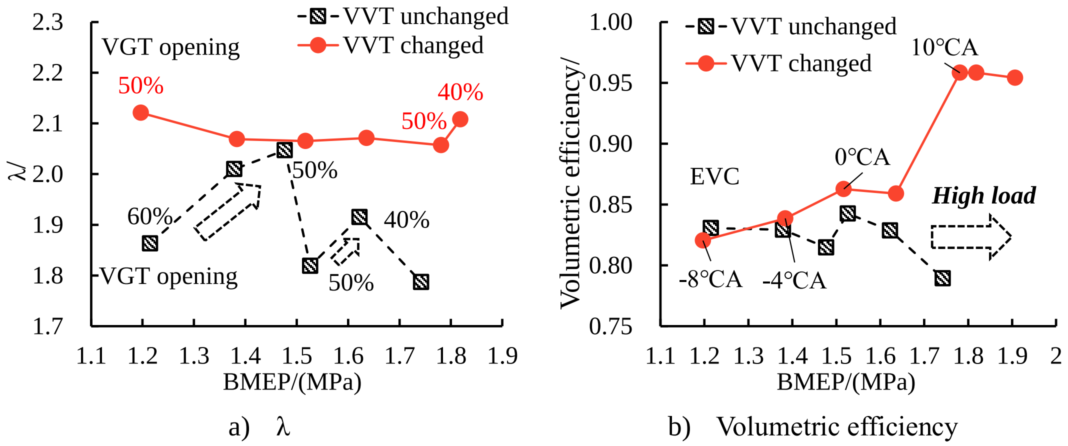


Figure 17 Parameters variation with changed or unchanged VVT settings at 2500 rpm

Figure 18 shows that the BTE with unchanged VVT is higher at medium-high loads. The BTE surpasses 42.4% as BMEP ranges from 1.52 MPa to 1.74 MPa. However, the maximum BTE reaches 41.6% when the EVC is located at 0°CA and it falls gradually to 37.6% subsequently. The results indicate that advanced EVC performs better at medium-high loads when considering BTE. In addition, the $NO_x$ emissions stay below approximately 50 ppm with unchanged VVT when the BMEP ranges from 1.21 MPa to 1.52 MPa. However, as the BMEP further increases, the $NO_x$ emissions dramatically rise to 1164 ppm. In contrast, the maximum with changed VVT is limited to 210 ppm at a BMEP of 1.82 MPa. Thus, the VVT settings are necessary to re-regulate at high loads to restrict $NO_x$ emissions.

The unchanged and changed exhaust valve timing is evaluated according to the weight of thermal efficiency and $NO_x$ emission and the results are displayed in Figure 19. The evaluation with unchanged VVT stays above 0.93 at medium and low loads, however, it significantly falls to 0.26 with the BMEP increases to 1.74 MPa. On the contrary, the evaluation with changed VVT shows its superiority at high loads though it decreases a little from 0.96 to 0.79. In addition, better exhaust valve timings are determined according to the evaluation comparison with different EVCs. For instance, the green dots in Figure 19 represent the evaluation with 10°CA of EVC, and they are lower than the red dots with 0°CA of EVC in the range from 1.51MPa to 1.63MPa of BMEP. This indicates the 0°CA EVC is the better one between these two exhaust valve timings.

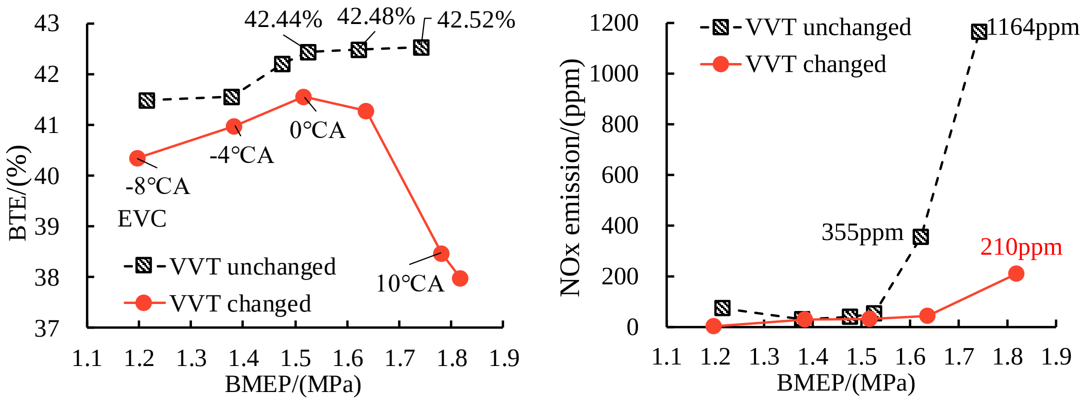


a) BTE b) NOx emission

Figure 18 BTE and $NO_x$ emission variation with changed or unchanged VVT settings at 2500 rpm

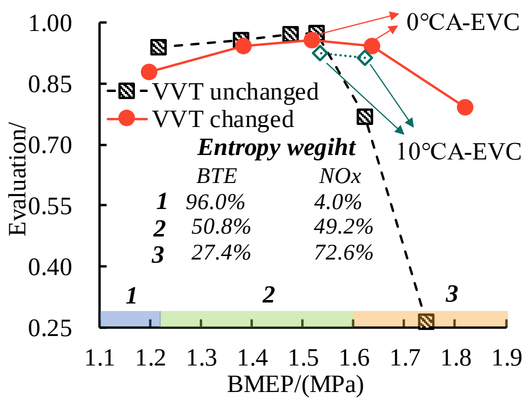


Figure 19 Evaluation with changed or unchanged VVT settings at different BMEP

The cylinder pressure shows that there is slight abnormal combustion in the hydrogen engine with unchanged VVT when the BMEP reaches 1.78 MPa, and λ reduces to 1.74. Figure 20 indicates a potential preignition occurred at the end of the compression stroke, leading to a significant rise in maximum cylinder pressure of 57%, which could damage the hydrogen engine. The further improvement of power will be constricted by such abnormal combustion. In summary, the sharp retardation of EVC is a result of balancing between thermal efficiency and $NO_x$ emissions. The advanced IVO and EVC are employed in the hydrogen engine to enhance BTE at medium-high loads until the $NO_x$ emission rises rapidly. Subsequently, the EVC is retarded sharply at high loads to improve volumetric efficiency and reduce $NO_x$ emissions. Furthermore, the retarded EVC can reduce the risk of abnormal combustion which has been observed with advanced EVC at high loads.

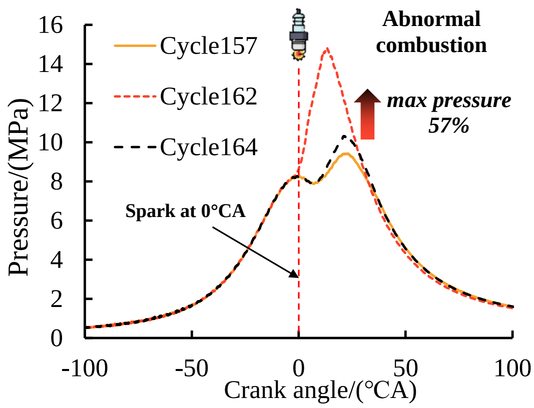


Figure 20 Abnormal combustion occuring at 1.78 MPa BMEP with unchanged VVT

The VVT settings of the hydrogen engine have been optimized with VGT opening control to achieve high power and high thermal efficiency. In addition, the $NO_x$ emissions are minimized as much as is possible. The results are displayed in Figure 21, and the hydrogen engine can achieve high thermal efficiency and power performance by coordinating VVT and VGT. As Figure 4 shows, the max torque and power reach 326.4 N·m at 2500 rpm and 124.8 kW at 4500 rpm respectively. The torque reaches 322.3 N·m at 1500 rpm, indicating a respectable low-speed performance. Furthermore, the max BTE reaches 42.57%. The results indicate that BTE considerably decreases when VVT settings are changed to pursue high power. Additionally, fair emission performance is achieved by optimizing VVT settings. The black island on Figure 21 represents the region with $NO_x$ emissions below 20 ppm, which contains nearly half of the whole operating map.

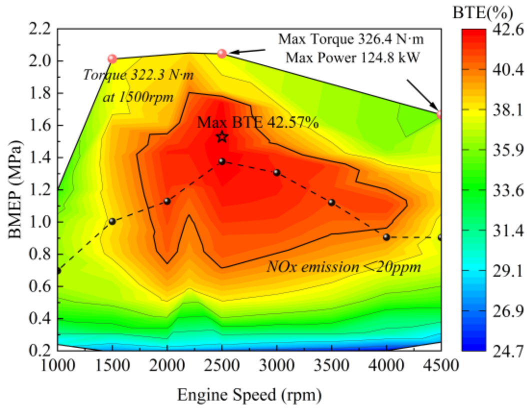


Figure 21 Operating map of the hydrogen engine

## 4. Conclusions

This research focuses on the optimization the performance of VVT on a 2.0 L DI $H_2$ICE over the whole operating map and conclusions are drawn as follows.

1. The Entropy Weight of thermal efficiency and $NO_x$ emissions are analyzed according to test results at different engine speeds and loads. The analysis shows that thermal efficiency is the primary indicator in optimizing VVT settings at medium-low loads, and the $NO_x$ emissions become the major indicator at high loads. The evaluation of VVT settings based on the entropy weights is a very helpful design approach.
2. VVT settings of the hydrogen engine are found to be distinct from those of the gasoline engine. Due to the characteristics of hydrogen and the intake pressure, there is a significant difference in airflow between the gasoline engine and the hydrogen engine. In addition, the lower exhaust back pressure controlled by the VGT opening also affects the VVT settings.
3. The intake valve timing strategy is studied. Advanced intake valve timing greatly improves the thermal efficiency. The optimal IVO is determined primarily based on the maximum BTE according to the Entropy Weight analysis, and a substantial retardation is necessary at high

speeds due to the greater air flow rate.

4. The exhaust valve timing strategy is also investigated. The EVC affects BTE because of pumping losses when the IVO is fixed. The EVC is a result of balancing thermal efficiency and $NO_x$ emissions and the evaluation is conducted based on the Entropy Weight of these two indicators to determine the optimal EVC. Advanced EVC is employed in the hydrogen engine to enhance BTE at medium loads. Subsequently, EVC is retarded sharply at high loads due to the significant increases in the Entropy Weight of $NO_x$ emissions and the improvement in volumetric efficiency.
5. VVT settings are optimized and employed in the hydrogen engine to improve performance. Maximum torque and power reach 326.4 N·m at 2500 rpm and 124.8 kW at 4500 rpm respectively. The torque reaches 322.3 N·m at 1500 rpm, indicating a respectable low-speed performance. The max BTE reaches 42.57%. Furthermore, $NO_x$ emissions are controlled under 20 ppm at nearly half of the engine operating map, resulting in fair emission performance.

## Acknowledgment

This study was supported by the China Postdoctoral Science Foundation (2023M730238) and Young Elite Scientists Sponsorship Program by CAST (2023QNRC001). This study was supported by the National Natural Science Foundation of China (Grant No.:52206228).

**Reference**

[1] Niu R, Yu X, Du Y, Xie H, Wu H, Sun Y. Effect of hydrogen proportion on lean burn performance of a dual fuel SI engine using hydrogen direct-injection. Fuel 2016;186:792–9. https://doi.org/10.1016/j.fuel.2016.09.021.

[2] Osipova KN, Zhang X, Sarathy SM, Korobeinichev OP, Shmakov AG. Ammonia and ammonia/hydrogen blends oxidation in a jet-stirred reactor: Experimental and numerical study. Fuel 2022;310:122202. https://doi.org/10.1016/j.fuel.2021.122202.

[3] Thawko A, Tartakovsky L. The Mechanism of Particle Formation in Non-Premixed Hydrogen Combustion in a Direct-Injection Internal Combustion Engine. Fuel 2022;327:125187. https://doi.org/10.1016/j.fuel.2022.125187.

[4] Teoh YH, How HG, Le TD, Nguyen HT, Loo DL, Rashid T, et al. A review on production and implementation of hydrogen as a green fuel in internal combustion engines. Fuel 2023;333:126525. https://doi.org/10.1016/j.fuel.2022.126525.

[5] Barış O, Güler İ, Yaşgül A. The effect of different charging concepts on hydrogen fuelled internal combustion engines. Fuel 2023;343:127983. https://doi.org/10.1016/j.fuel.2023.127983.

[6] Desantes JM, Molina S, Novella R, Lopez-Juarez M. Comparative global warming impact and NOX emissions of conventional and hydrogen automotive propulsion systems. Energy Conversion and Management 2020;221:113137. https://doi.org/10.1016/j.enconman.2020.113137.

[7] Desantes JM, Novella R, Pla B, Lopez-Juarez M. Impact of fuel cell range extender powertrain design on greenhouse gases and NOX emissions in automotive applications. Applied Energy 2021;302:117526. https://doi.org/10.1016/j.apenergy.2021.117526.

[8] Gong C, Li Z, Yi L, Liu F. Experimental investigation of equivalence ratio effects on combustion and emissions characteristics of an H2/methanol dual-injection engine under different spark timings. Fuel 2020;262:116463. https://doi.org/10.1016/j.fuel.2019.116463.

[9] Verhelst S, Wallner T. Hydrogen-fueled internal combustion engines. Progress in Energy and Combustion Science 2009;35:490–527. https://doi.org/10.1016/j.pecs.2009.08.001.

[10] Verhelst S. Recent progress in the use of hydrogen as a fuel for internal combustion engines. International Journal of Hydrogen Energy 2014;39:1071–85. https://doi.org/10.1016/j.ijhydene.2013.10.102.

[11] Wickham D, Hawkes A, Jalil-Vega F. Hydrogen supply chain optimisation for the transport sector – Focus on hydrogen purity and purification requirements. Applied Energy 2022;305:117740. https://doi.org/10.1016/j.apenergy.2021.117740.

[12] Nguyen D, Turner JWG. Effect of nitric oxide on the performance and emissions of a hydrogen-fueled HCCI engine. Fuel 2023;349:128611. https://doi.org/10.1016/j.fuel.2023.128611.

[13] Gong C, Zhang Z, Sun J, Liu F. Optimization on timings of injection and spark of a high compression-ratio stratified-charge methanol engine under ultra-lean burn. Fuel 2021;285:119227. https://doi.org/10.1016/j.fuel.2020.119227.

[14] Dimitriou P, Tsujimura T. A review of hydrogen as a compression ignition engine fuel. International Journal of Hydrogen Energy 2017;42:24470–86. https://doi.org/10.1016/j.ijhydene.2017.07.232.

[15] Sarıkoç S. Environmental and enviro-economic effect analysis of hydrogen-methanol-gasoline addition into an SI engine. Fuel 2023;344:128124. https://doi.org/10.1016/j.fuel.2023.128124.

[16] Yu X, Du Y, Sun P, Liu L, Wu H, Zuo X. Effects of hydrogen direct injection strategy on characteristics of lean-burn hydrogen–gasoline engines. Fuel 2017;208:602–11. https://doi.org/10.1016/j.fuel.2017.07.059.

[17] Wang B, Yang C, Wang H, Hu D, Wang Y. Effect of Diesel-Ignited Ammonia/Hydrogen mixture fuel combustion on engine combustion and emission performance. Fuel 2023;331:125865. https://doi.org/10.1016/j.fuel.2022.125865.

[18] Cunanan C, Tran M-K, Lee Y, Kwok S, Leung V, Fowler M. A Review of Heavy-Duty Vehicle Powertrain Technologies: Diesel Engine Vehicles, Battery Electric Vehicles, and Hydrogen Fuel Cell Electric Vehicles. Clean Technol 2021;3:474–89. https://doi.org/10.3390/cleantechnol3020028.

[19] Novella R, García A, Gomez-Soriano J, Fogué-Robles Á. Exploring dilution potential for full load operation of medium duty hydrogen engine for the transport sector. Applied Energy 2023;349:121635. https://doi.org/10.1016/j.apenergy.2023.121635.
[20] Bao L, Sun B, Luo Q, Li J, Qian D, Ma H, et al. Development of a turbocharged direct-injection hydrogen engine to achieve clean, efficient, and high-power performance. Fuel 2022;324:124713. https://doi.org/10.1016/j.fuel.2022.124713.
[21] Lu C, Chen W, Zuo Q, Kou C, Wang H, Xiao G, et al. Numerical investigation on gaseous fuel injection strategies on combustion characteristics and NO emission performance in a pure hydrogen engine. Fuel 2024;363:130911. https://doi.org/10.1016/j.fuel.2024.130911.
[22] Özyalcin C, Sterlepper S, Roiser S, Eichlseder H, Pischinger S. Exhaust gas aftertreatment to minimize NOX emissions from hydrogen-fueled internal combustion engines. Applied Energy 2024;353:122045. https://doi.org/10.1016/j.apenergy.2023.122045.
[23] Yuan Z, Fu J, Liu Q, Ma Y, Zhan Z. Quantitative study on influence factors of power performance of variable valve timing (VVT) engines and correction of its governing equation. Energy 2018;157:314–26. https://doi.org/10.1016/j.energy.2018.05.135.
[24] Kim S, Park C, Jang H, Kim C, Kim Y. Effect of boosting on a performance and emissions in a port fuel injection natural gas engine with variable intake and exhaust valve timing. Energy Reports 2021;7:4941–50. https://doi.org/10.1016/j.egyr.2021.07.073.
[25] Shu J, Fu J, Zhao D, Liu J, Ma Y, Deng B, et al. Numerical investigation on the effects of valve timing on in-cylinder flow, combustion and emission performance of a diesel ignition natural gas engine through computational fluid dynamics. Energy Conversion and Management 2019;198:111786. https://doi.org/10.1016/j.enconman.2019.111786.
[26] Basaran HU, Ozsoysal OA. Effects of application of variable valve timing on the exhaust gas temperature improvement in a low-loaded diesel engine. Applied Thermal Engineering 2017;122:758–67. https://doi.org/10.1016/j.applthermaleng.2017.04.098.
[27] Lee J, Lee K, Lee J, Anh B. High power performance with zero NOx emission in a hydrogen-fueled spark ignition engine by valve timing and lean boosting. Fuel 2014;128:381–9. https://doi.org/10.1016/j.fuel.2014.03.010.
[28] Xin G, Ji C, Wang S, Hong C, Meng H, Yang J, et al. Experimental study of the effect of variable valve timing on hydrogen-enriched ammonia engine. Fuel 2023;344:128131. https://doi.org/10.1016/j.fuel.2023.128131.
[29] Verhelst S, Demuynck J, Sierens R, Huyskens P. Impact of variable valve timing on power, emissions and backfire of a bi-fuel hydrogen/gasoline engine. International Journal of Hydrogen Energy 2010;35:4399–408. https://doi.org/10.1016/j.ijhydene.2010.02.022.
[30] Park C, Park W, Kim Y, Choi Y, Lim B. Effect of Valve Timing and Excess Air Ratio on Torque in Hydrogen-Fueled Internal Combustion Engine for UAV. Energies 2019;12:771. https://doi.org/10.3390/en12050771.
[31] Dennis PA, Dingli RJ, Abbasi Atibeh P, Watson HC, Brear MJ, Voice G. Performance of a Port Fuel Injected, Spark Ignition Engine Optimised for Hydrogen Fuel, 2012, p. 2012-01–0654. https://doi.org/10.4271/2012-01-0654.
[32] Gao J, Wang X, Song P, Tian G, Ma C. Review of the backfire occurrences and control strategies for port hydrogen injection internal combustion engines. Fuel 2022;307:121553. https://doi.org/10.1016/j.fuel.2021.121553.
[33] Reichel TG, Paschereit CO. Interaction mechanisms of fuel momentum with flashback limits

in lean-premixed combustion of hydrogen. International Journal of Hydrogen Energy 2017;42:4518–29. https://doi.org/10.1016/j.ijhydene.2016.11.018.
[34] Wang L, Yang Z, Huang Y, Liu D, Duan J, Guo S, et al. The effect of hydrogen injection parameters on the quality of hydrogen–air mixture formation for a PFI hydrogen internal combustion engine. International Journal of Hydrogen Energy 2017;42:23832–45. https://doi.org/10.1016/j.ijhydene.2017.04.086.
[35] Xu P, Ji C, Wang S, Cong X, Ma Z, Tang C, et al. Effects of direct water injection on engine performance in engine fueled with hydrogen at varied excess air ratios and spark timing. Fuel 2020;269:117209. https://doi.org/10.1016/j.fuel.2020.117209.
[36] Bao L, Sun B, Luo Q. Optimal control strategy of the turbocharged direct-injection hydrogen engine to achieve near-zero emissions with large power and high brake thermal efficiency. Fuel 2022;325:124913. https://doi.org/10.1016/j.fuel.2022.124913.
[37] Ji C, Hong C, Wang S, Xin G, Meng H, Yang J, et al. Evaluation of the variable valve timing strategy in a direct-injection hydrogen engine with the Miller cycle under lean conditions. Fuel 2023;343:127932. https://doi.org/10.1016/j.fuel.2023.127932.
[38] Hong C, Ji C, Wang S, Xin G, Wang Z, Meng H, et al. Assessment of a synergistic control of intake and exhaust VVT for airflow exchange, combustion, and emissions in a DI hydrogen engine. International Journal of Hydrogen Energy 2023;48:20495–506. https://doi.org/10.1016/j.ijhydene.2023.03.002.
[39] Hong C, Ji C, Wang S, Xin G, Wang Z, Meng H, et al. An experimental study of various load control strategies for an ammonia/hydrogen dual-fuel engine with the Miller cycle. Fuel Processing Technology 2023;247:107780. https://doi.org/10.1016/j.fuproc.2023.107780.
[40] Xu G, Jia M, Li Y, Chang Y, Wang T. Potential of reactivity controlled compression ignition (RCCI) combustion coupled with variable valve timing (VVT) strategy for meeting Euro 6 emission regulations and high fuel efficiency in a heavy-duty diesel engine. Energy Conversion and Management 2018;171:683–98. https://doi.org/10.1016/j.enconman.2018.06.034.
[41] Xu G, Jia M, Li Y, Chang Y, Liu H, Wang T. Evaluation of variable compression ratio (VCR) and variable valve timing (VVT) strategies in a heavy-duty diesel engine with reactivity controlled compression ignition (RCCI) combustion under a wide load range. Fuel 2019;253:114–28. https://doi.org/10.1016/j.fuel.2019.05.020.
[42] Jia G, Gao S, Shu X, Ren B, Zhang B, Ma G, et al. Multi-objective optimization of emission parameters of a diesel engine using oxygenated fuel and pilot injection strategy based on RSM-NSGA III. Energy 2024;293:130661. https://doi.org/10.1016/j.energy.2024.130661.